Comprehensive Status Report: November 18, 2004

OTRC Project Title: Mitigating Greenwater Damage Through Design
MMS Project 441 TO 85385
PI: Kuang-an Chang, Hamn-Ching Chen, Richard Mercier
MMS COTR: A. Konczvald

This report provides a comprehensive summary of the research completed in all prior Phases of this project (September 2002 – August 2004), and describes research being done in the present Phase (September 2004 – August 2005) to complete this project.

Mitigating Greenwater Damage Through Design

Kuang-An Chang, Hamn-Ching Chen, and Richard S. Mercier

Project Objective & Description

Greenwater damage to floating structures results from high pressures and loads that occur when wave crests inundate the structure far above the waterline in areas not designed to withstand such pressures. Greenwater damage is the result of unique combinations of vessel motions and incident wave conditions, e.g. roll, pitch and yaw of a turret-moored FPSO in hurricane seas. The interactions between extreme waves and floating structures will be studied both analytically and experimentally to better understand the complex flows around and over a structure, and the resulting impact loads and pressures that can cause damage. These results will be combined with capabilities to predict vessel motions in order to develop design guidance that will allow designers to avoid or minimize greenwater through design (e.g., hull shape, protective appurtenances, and strategic reinforcement). In addition to ship-shaped FPSO's, the project will also consider other structure geometries such as spars or TLP's.

Progress

Summary A fixed 2D rectangular structure based on the dimensions of a typical TLP (1:168 scaled down) was tested in the laboratory flume using extreme waves breaking and impinging on the structure with greenwater. Velocity fields in the vicinity of the structure, including greenwater, were measured over the entire impinging process using the traditional particle image velocimetry (PIV) technique and a newly developed PIV method that directly tracks the air bubbles. Detailed measurements for plunging wave impinging on the structure with a large air pocket are completed. The results are compared with the 1D (depth averaged with only the horizontal velocity) linear solution of dam-breaking theory, which has been widely used to simulate greenwater effect. Preliminary results show that the theory seems to over predict the velocity in the initial stage of greenwater due to wave impinging and overtopping, while under predict the velocity after the initial stage. The discrepancy may be contributed, by examining the PIV velocity maps, from the vertical component of velocity on the deck that is significant at the initial stage but quickly dies down afterward. Future work will be to parameterize the greenwater effect from the PIV velocity maps and modify the existing prediction model. The void fraction of the greenwater will also be measured.

A Reynolds-Averaged Navier-Stokes (RANS) numerical method has been developed in conjunction with a chimera domain decomposition approach for simulation of the greenwater effects and impact loads on floating platforms. Time-domain simulations of wave runup were performed for fixed platforms subjected to regular waves. In these simulations, the boundary-fitted platform grid remains fixed, while the free surface and basin grids were updated every time step to follow the movement of nonlinear free surface waves. This enables us to accurately resolve the body boundary layer and wakes without undesirable grid distortions even in the presence of greenwater on the deck. New absorbing beach techniques were developed for both the wavemaker and downstream boundaries to facilitate the long duration simulations without unphysical wave reflections from computational domain boundary. The predicted wave elevation and velocity field are in

good agreement with the corresponding PIV data for 2D rectangular platform. The method has also been extended successfully for simulation of wave runup around three-dimensional offshore structures.

A more detailed summary of the **Experimental Results** and the **Numerical Simulation Results** follows.

Experimental Results The experiments were carried out in a wave flume that is 35 m long, 0.9 m wide, and 1.2 m height. A flap-type wavemaker is installed at one end of the flume while the other end is a 1:5.5 sloping beach with a layer of dissipating material on top to reduce reflection. The test model is mounted at 21 m from the wavemaker. Figure 1 depicts the setup of the experiments.

The sketch of the model is shown in Figure 2. The model is 0.31 m height, 0.15 long, and 0.90 m wide (the same as that of the flume) with a draft of 0.20 m. Velocity measurements cover the frontal part of the structure using traditional PIV and the entire structure using the newly developed PIV method (thereafter called "bubble PIV" due to its principle of tracking air bubbles). The coordinate system (x, z) has an original at the frontal edge of the structure and the still water level. Figure 3 shows the incoming wave train measured by a wave gauge located at 5 m from the wavemaker (x = -16 m). Water depth was kept constant at 0.80 m. The primary wave (the largest one) which later breaks and impinges on the structure has a wave period of 1.3 s and wave height of 17 cm. Figure 4 shows the wave gauge measurement at the frontal edge of the structure (x = 0). The maximum wave height shown in the figure is 24 cm.

The traditional PIV technique did not work well here due to the existence of air bubbles in the highly aerated region close to and on top of the structure. The problem becomes severe when the breaking waves are plunging breakers. The reason is that the large amount of air bubbles scatters the laser light and result in saturated images captured by the camera. We since alternated our approach by replacing the laser with halogen light and carefully adjusting the camera aperture (the f-stop) so the depth of view is limited to only around 10 cm inside the flume. Since the camera is located at a distance 3 m away from the focal plane, the error due to the uncertainty of the object (bubbles here) in the depth of view is approximately one-half of the depth of view divided by the distance. This gives an error of (5 cm)/(3 m) that is less than 2%. The setup of the "bubble" PIV is depicted in Figure 5.

The measured velocity fields from this alternated approach are successful and shown in Figure 6. In the figure, the breaking wave impinges on the structure and creates green water. Initially at the wave front velocity changes from mainly horizontal to vertical after hitting the structure (Figures 6(a - c)) and the water continues to move upward until later the wave momentum pushes the front to move forward onto the deck. The water does not touch the deck surface until the instant in Figures 6(e - f). The horizontal velocity on the deck is also very small initially until the water starts to touch the deck. In Figures 6(g - h) the wave velocity becomes completely horizontal. This could create a large horizontal force exerting to any objects on the deck due to its large momentum. Since the deck is not long (see the plot on Figure 6(a)), the water on top of the deck passes the deck and moves downward back to the "ocean" quickly at the rear edge of the deck as seen in Figures 6(i - l). The water level on the deck also quickly reduces.

The measured maximum horizontal velocity of the breaking wave in front of the structure is shown in Figure 7. The figure clearly indicates that the wave particle velocity is slightly greater than the wave celerity, C, before reaching the structure. Subsequently the maximum horizontal velocity reaches 1.5C right before

hitting the structure. After the plunging jet hitting and overtopping onto the structure, the velocity is significantly reduced to around one-half of the wave celerity.

Figure 8 shows the horizontal velocity component of greenwater on the deck of the structure. The measured maximum horizontal velocity is around 0.7*C*. The lines are corresponding solution from the dam-breaking theory. The preliminary comparison shows, if matching the timing at the moment when the wave starts to touch the surface of the deck (corresponding to instant in Figure 8(f)), the linear solution seems to under predict the greenwater velocity. However, before the moment of wave touching the deck surface, the linear solution gives much higher velocity. We therefore conclude that the dam-breaking solution over predicts the greenwater velocity before the deck has greenwater, and under predict the velocity when the green water exists on the deck.

Numerical Simulation Results A Reynolds-Averaged Navier-Stokes (RANS) numerical method has been developed in conjunction with the chimera domain decomposition approach to simulate the wave runup around offshore structures. Comparisons were made between the numerical predictions and PIV measurements for wave runup on two-dimensional platform to facilitate a detailed validation of the chimera RANS method. The method was then generalized to three-dimensions for time-domain simulation of wave runup around single and multiple cylinders.

In the present chimera domain decomposition approach for platform wave runup simulation, the solution domain is divided into several computational blocks as shown in Figure 9 to provide appropriate resolution of the platform boundary layers, wakes, as well as the nonlinear free surface waves. Note that the platform grid covers the entire platform surface including the dry deck area. The free surface grid blocks are updated every time step to follow the instantaneous free surface wave elevation. In addition, nonlinear free surface boundary conditions are imposed on the exact free surface for accurate prediction of the fully nonlinear wave field. It should also be noted that the platform grid remains fixed during the entire simulation even though the submerged section changes with instantaneous wave elevation. This not only simplifies the grid-generation process, but also eliminates undesirable grid distortion which typically occurs in the simulation of large amplitude wave motions.

Simulations were performed for the wave runup on the two-dimensional platform used in the above experimental study with two different incident wave heights of H = 0.115 m and 0.175 m, respectively. Figure 10 shows the computed free surface wave elevation and pressure contours at t/T = 18.375, 18.625, and 18.875, respectively. The superposition and cancellation of the incident and reflected waves at different time instants can be clearly seen from this figure. For long-duration simulations over many wave periods, the wave reflected by the platform will propagate back to the wavemaker boundary and interfere with the incident wave field. In the present study, a new absorbing beach approach has been implemented to prevent the reflected wave from reaching the wavemaker boundary. In this new absorbing beach approach, an additional computational block representing the wave tank was used to allow concurrent computation of the incident wave field without the presence of the offshore structure. This enables us to determine the exact patterns of the reflected wave since both wave fields with and without the structure were computed simultaneously at every time step. The present simulation results clearly demonstrated the effectiveness of

the new absorbing beach approach as the simulation was continued for more than 20 wave periods without any distortion in incident wave field.

Figure 11 shows the predicted velocity vectors and the corresponding vorticity contours at t/T = 18.25 and 18.75, respectively. At t/T = 18.25, the wave-induced current is moving downward and produces a strong counterclockwise vortex on the platform bottom surface adjacent to the weather side corner. Another weaker counterclockwise vortex was also observed on the lee side. At t/T = 18.75, the current reversed direction and a pair of clockwise vortices were induced around the sharp platform corners. It is also worthwhile to note that the water elevation on the lee side of the platform changes only slightly since the platform draft is relatively deep with negligible wave transmission.

Calculations were also performed for the higher wave case with an incident wave height H = 0.175 m. Figure 12 shows the predicted free surface elevation and pressure contours for the higher incident wave case at t/T = 21.27, 21.52, and 21.77, respectively. The corresponding vorticity contours and velocity vector plots are also shown in Figure 13 to provide a more detailed understanding of the wave-induced flow field around the platform. At t/T = 21.27, the wave runup is very close to the platform deck. However, no greenwater was observed either in the experiment or the simulation. In general, the wave-induced vorticity field is considerably stronger than that observed earlier for the H = 0.115 m case.

For completeness, comparisons were made between the numerical results and the corresponding PIV measurement data to provide a detailed assessment on the predictive capability of the present chimera RANS method. Figure 14 shows the predicted and measured velocity field at eight different time instants over one wave period. It is clearly seen that the numerical results are in close agreement with the corresponding experimental data for the H = 0.175 m case. Similar level of agreement was also observed for the H = 0.115 m case. These results clearly demonstrate the capability of the present chimera RANS method for accurate prediction of the wave runup around offshore platforms.

After successful validations of the chimera RANS method for two-dimensional platform configuration, the method was further generalized for time-domain simulation of wave runup around more practical three-dimensional configurations. Figures 15-17 shows the predicted wave patterns and free surface pressure contours around single and multiple circular cylinders. The predicted wave elevations in front of the cylinder are in good agreement with the available experimental data.

Present Work

The focus of the 2004-2005 numerical simulation tasks is to develop a more general chimera domain decomposition approach for time-domain simulation of greenwater effects on offshore platforms. A new free surface tracking technique will be incorporated to determine the water and air interface. Simulations will be performed for two-dimensional platform model and compared with the corresponding PIV measurements to assess the predictive capability of the chimera RANS method for greenwater predictions.

Reports & Publications

Ryu, Y. & Chang, K.-A., “Extreme waves impinging on an offshore structure.” Civil Engineering in the Oceans VI Conference, Baltimore, Maryland, October 20-22, 2004.

Chen, H.C., Yu, K. and Chen, S.Y., “Simulation of wave runup around offshore structures by a chimera domain decomposition approach,” Civil Engineering in the Oceans VI Conference, Baltimore, Maryland, October 20-22, 2004.

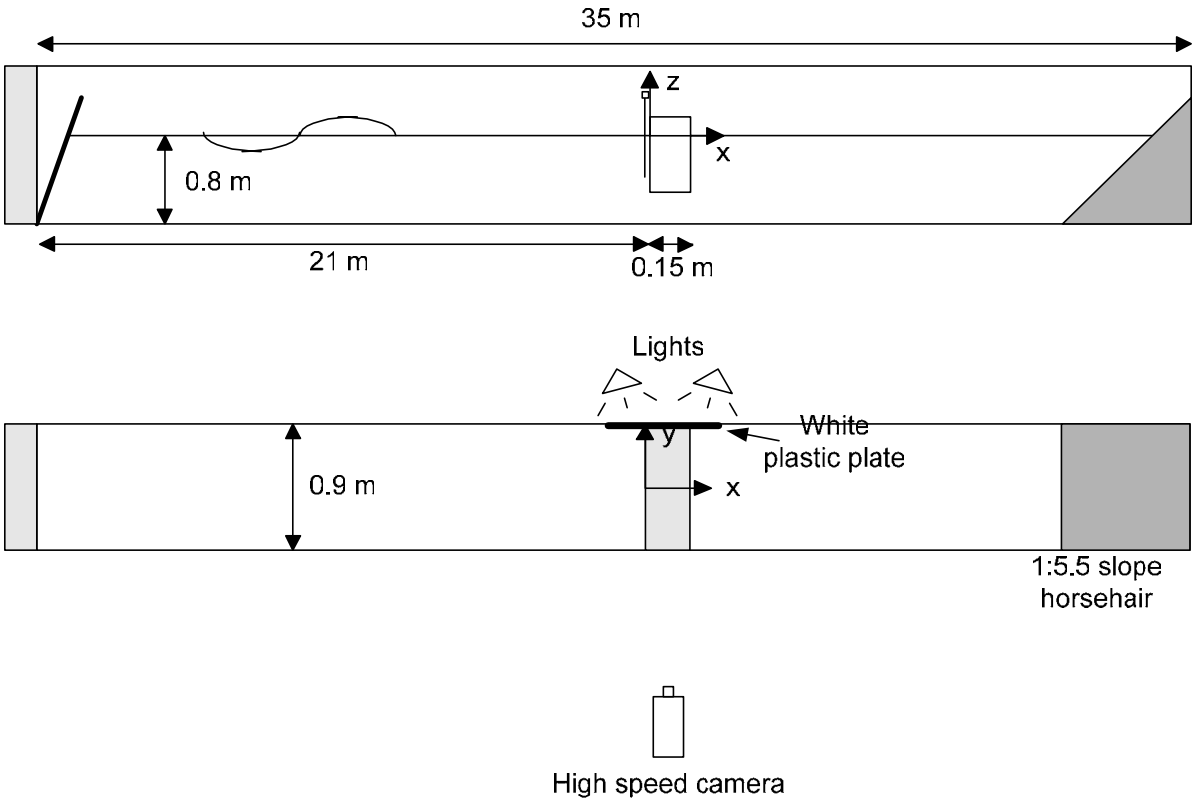

Figure 1: Experimental Setup. Upper panel: side view; lower panel: top view.

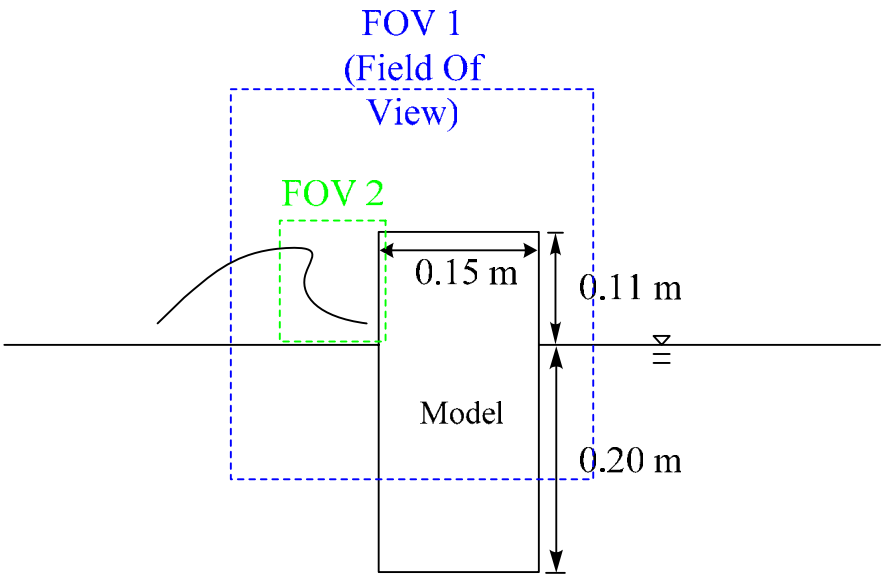

Figure 2: Sketch of the structure and PIV fields of view (FOV)

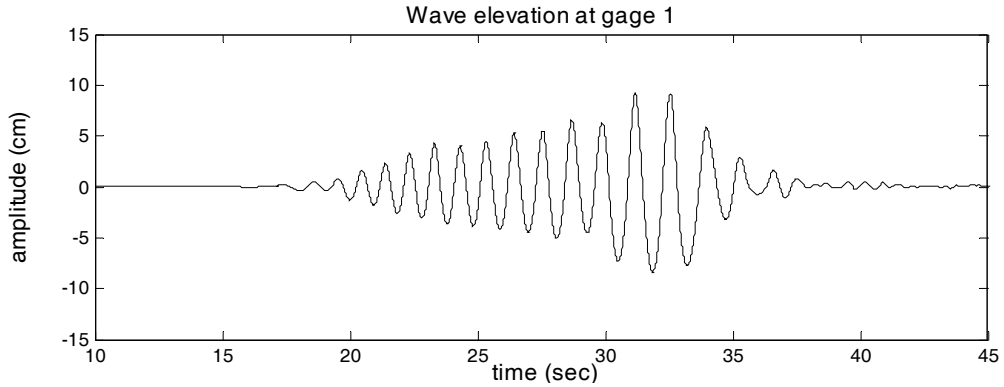

Figure 3: Wave gauge surface profile measurement at x = -16 m

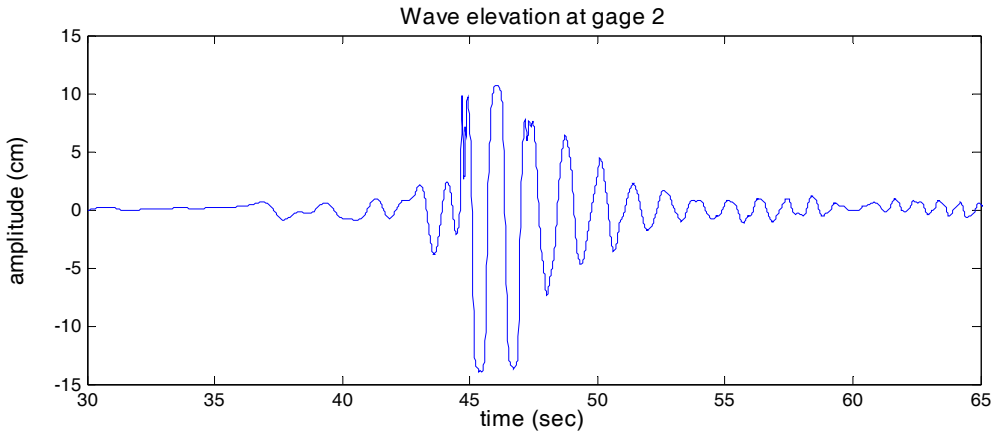

Figure 4: Wave gauge surface profile measurement at x = 0

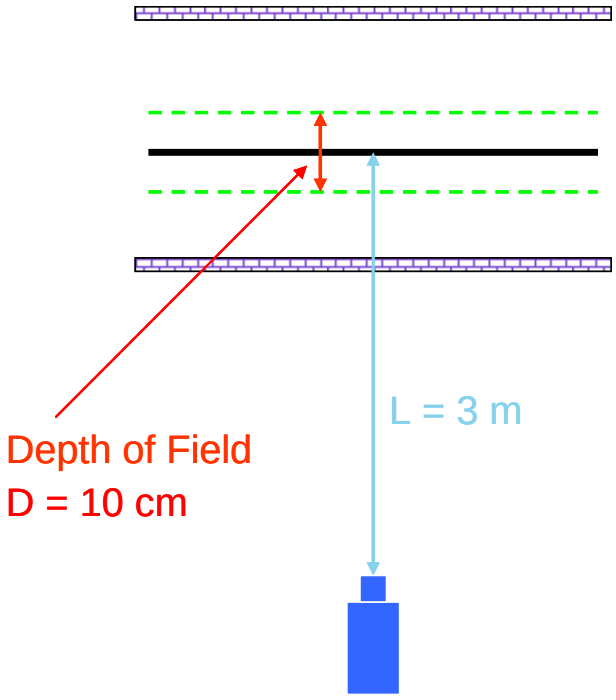

Figure 5: Setup of the "bubble" PIV system

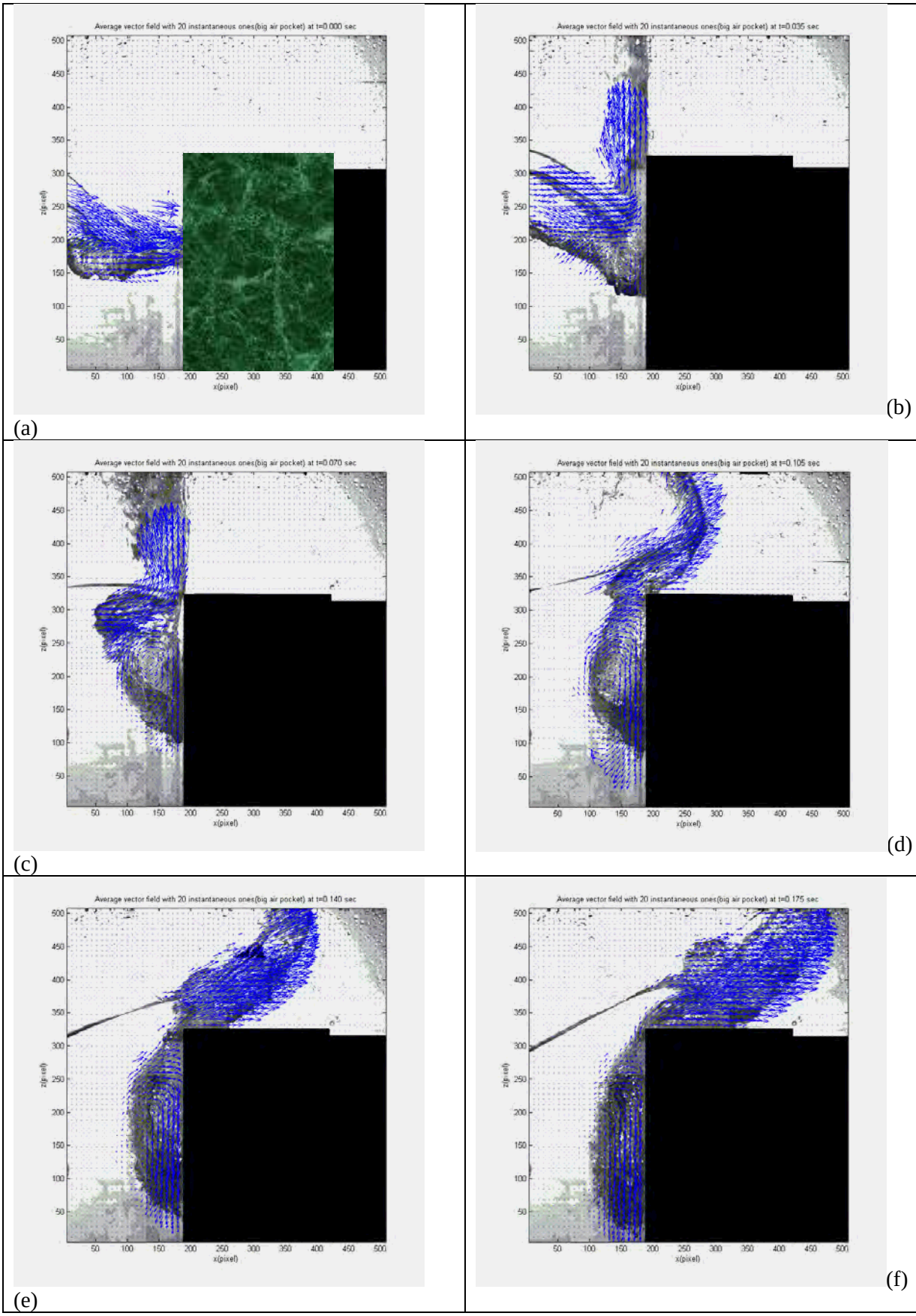

Figure 6: Bubble PIV velocity maps

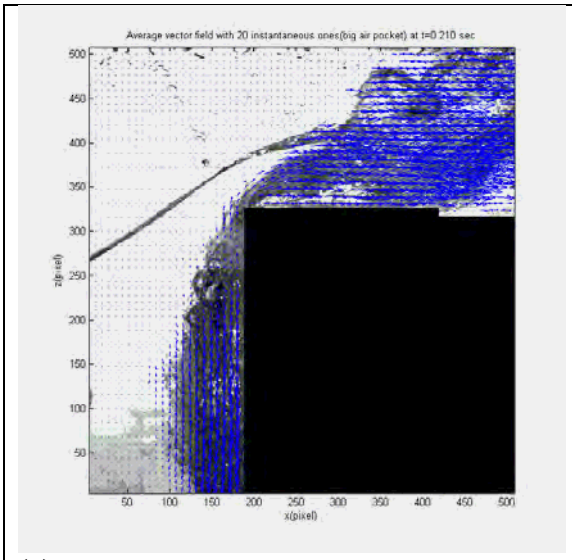

(g)

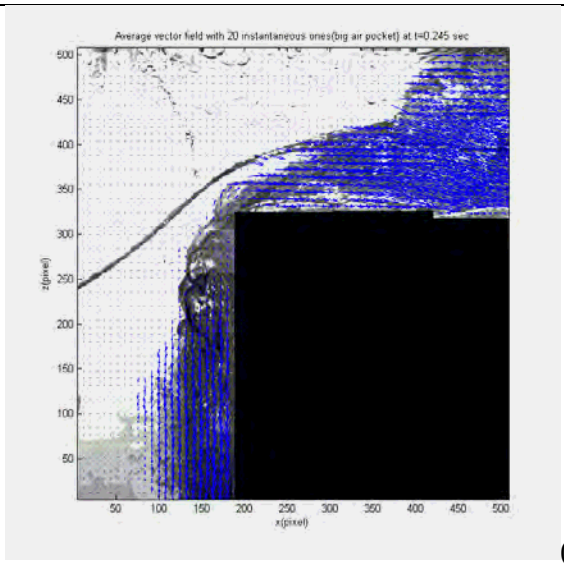

(h)

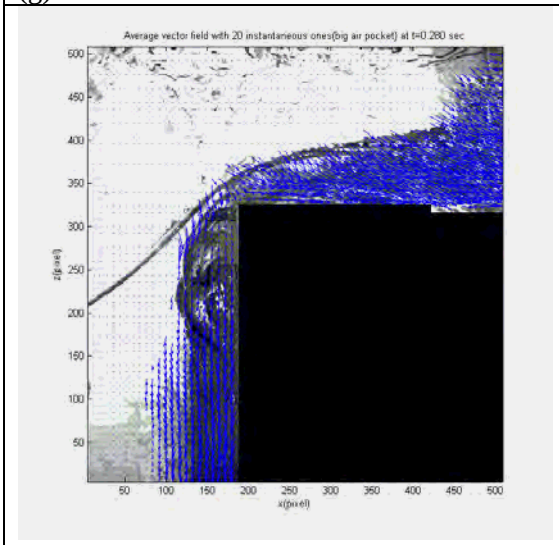

(i)

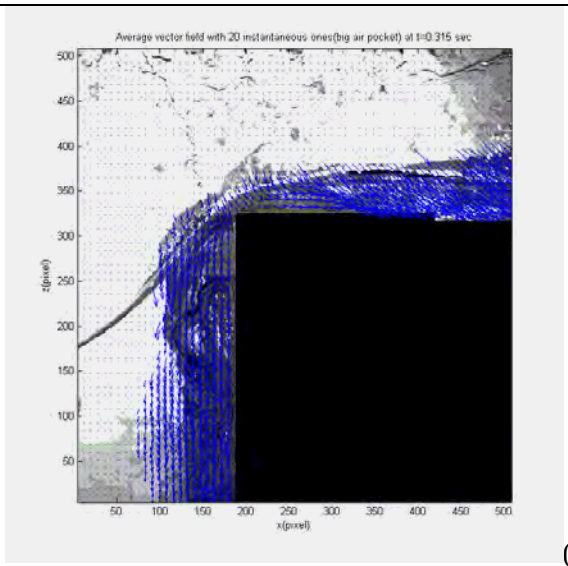

(j)

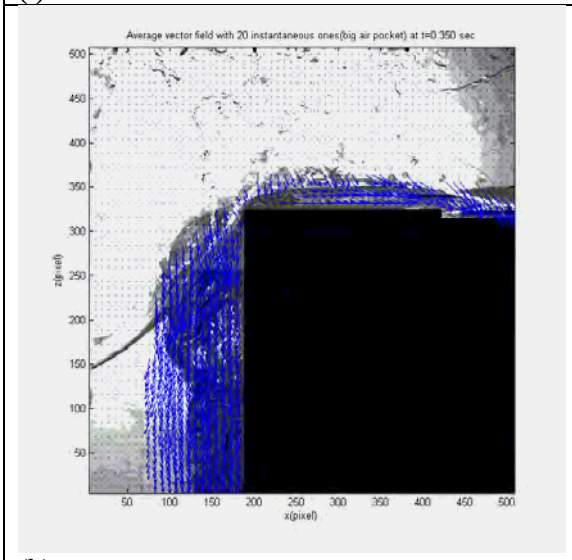

(k)

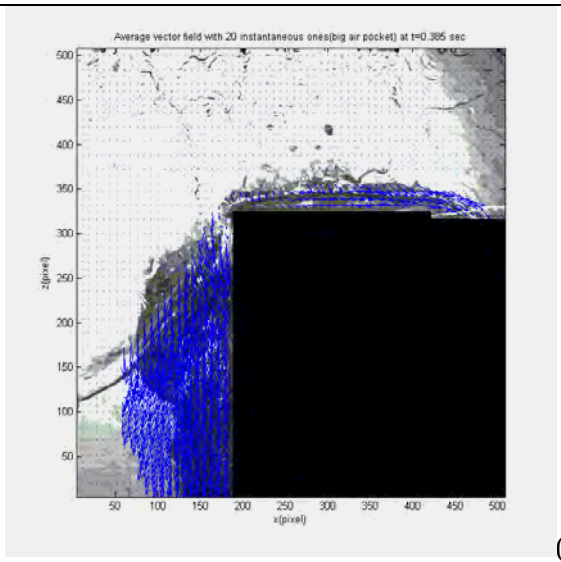

(l)

Figure 6: Continued

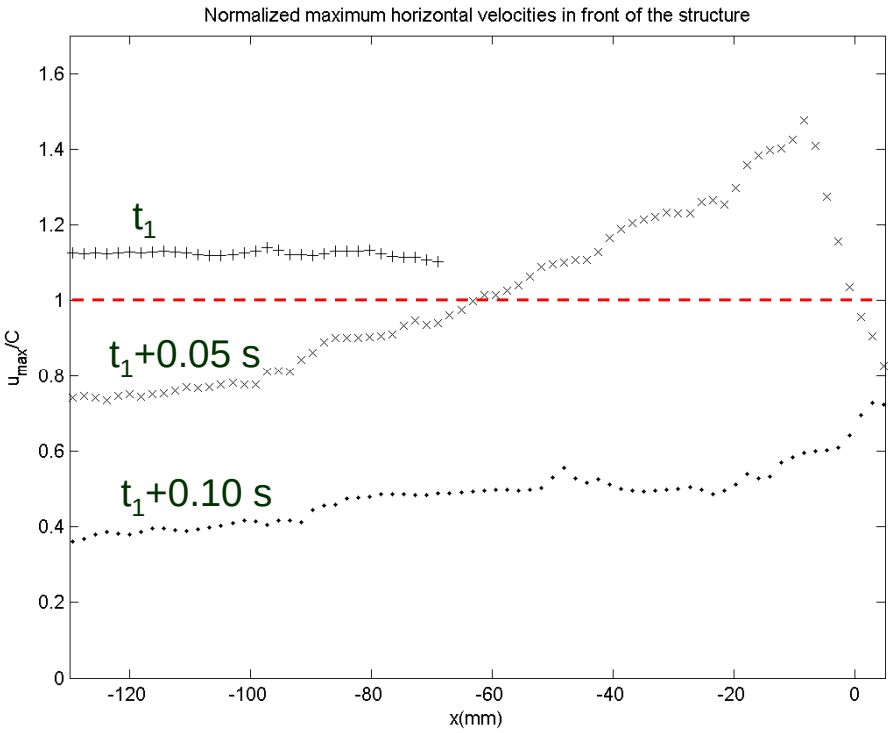

Figure 7: Maximum horizontal velocity in front of the structure

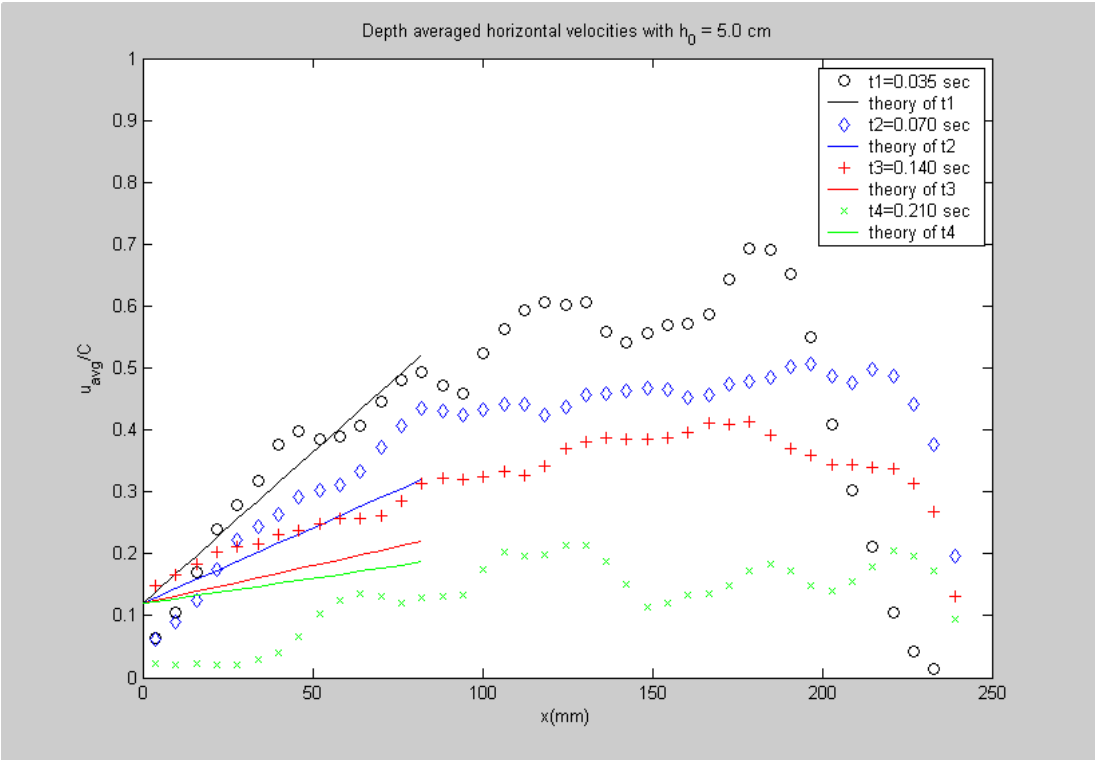

Figure 8: Greenwater velocity on the deck: Comparison between dam-breaking theory and measurement.

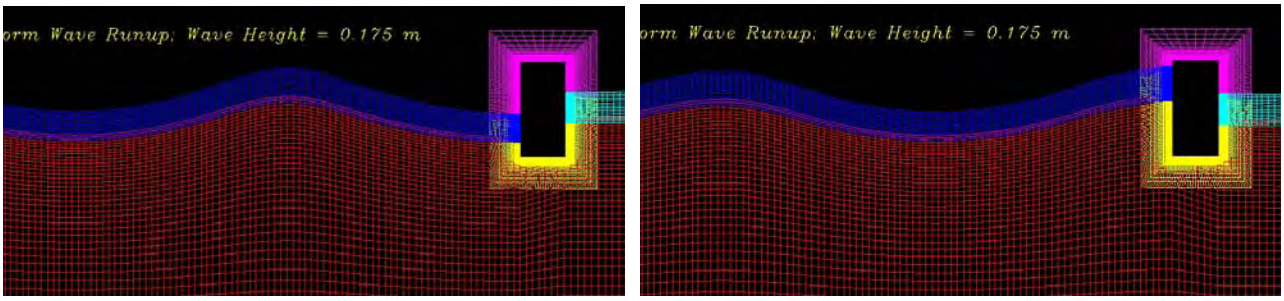

Figure 9: Chimera grid structure for time-domain simulation of wave runup.

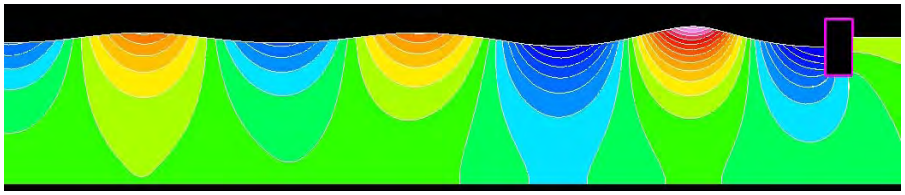

(a) *t/T* = 18.375

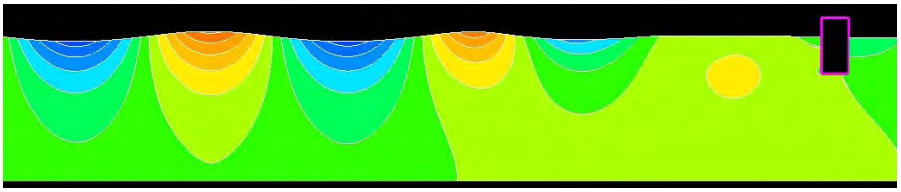

(b) *t/T* = 18.625

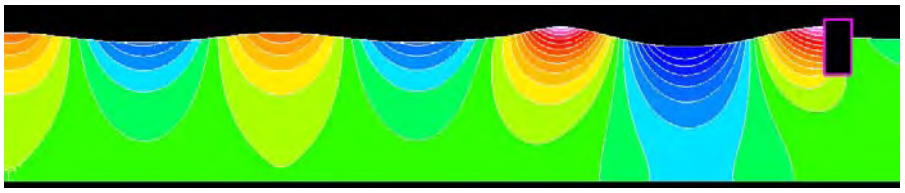

(c) *t/T* = 18.875

Figure 10: Wave elevation and pressure contours; incident wave height *H* = 0.115m.

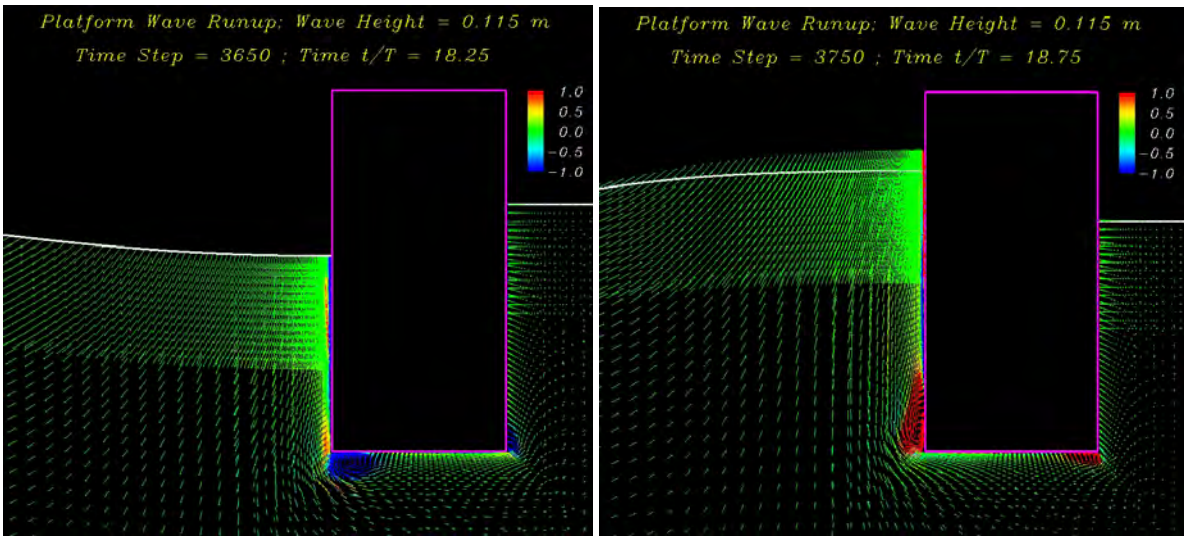

(a) *t/T* = 18.25 **(b) *t/T* = 18.75**

Figure 11: Velocity vectors and vorticity contours around the platform; *H* = 0.115 m.

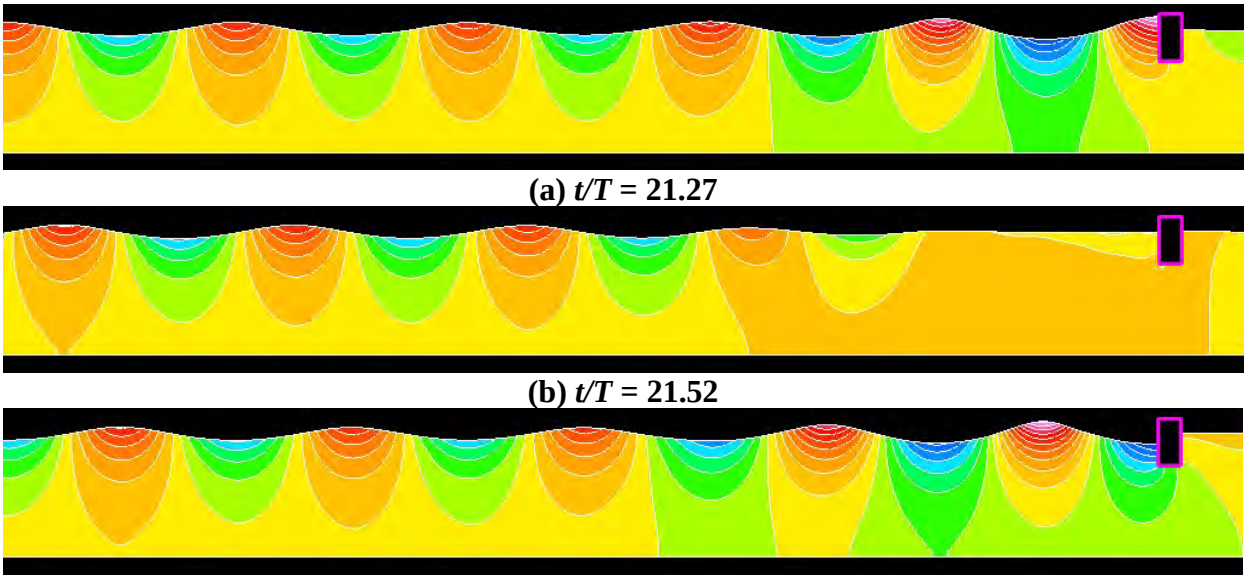

(a) *t/T* = 21.27

(b) *t/T* = 21.52

(c) *t/T* = 21.77

Figure 12: Wave elevation and pressure contours; incident wave height *H* = 0.175m.

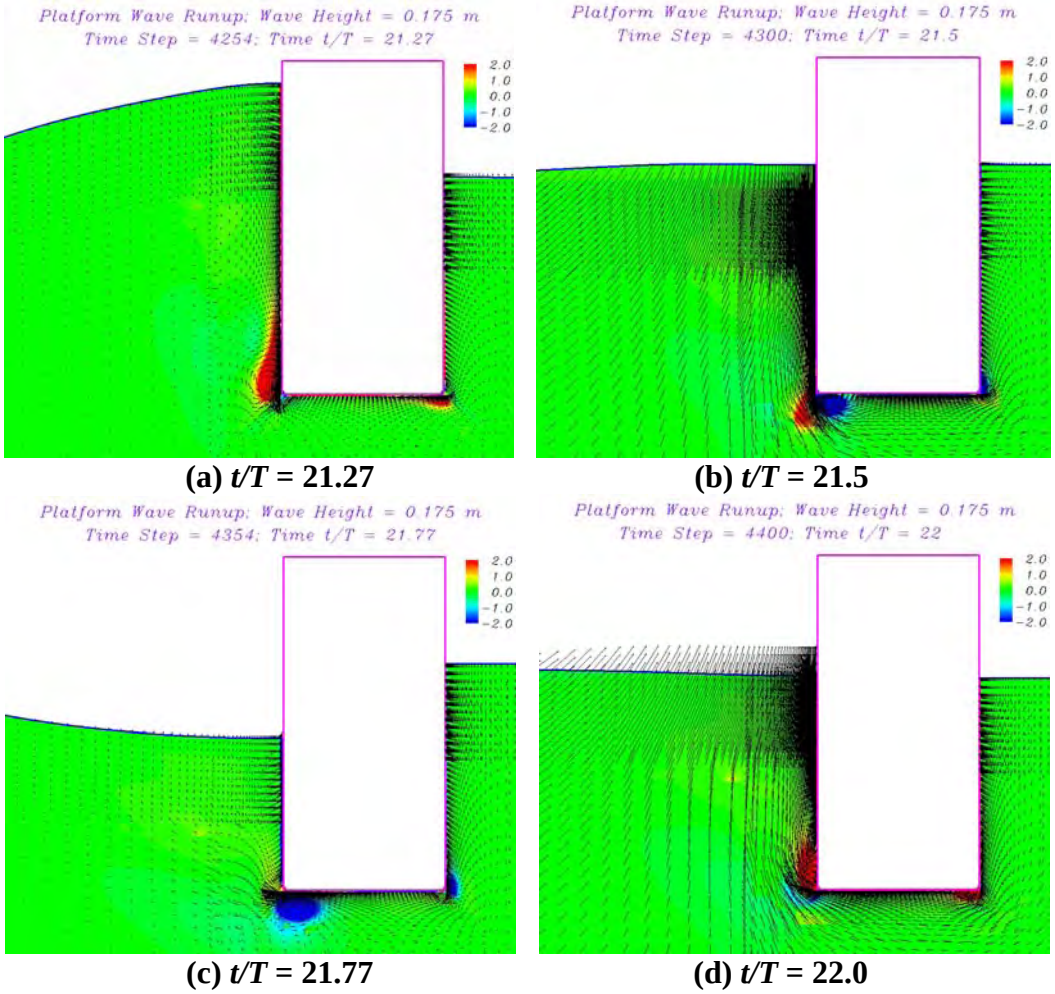

(a) *t/T* = 21.27 **(b) *t/T* = 21.5**

(c) *t/T* = 21.77 **(d) *t/T* = 22.0**

Figure 13: Vector vectors and Vorticity contours around the platform; *H* = 0.175 m.

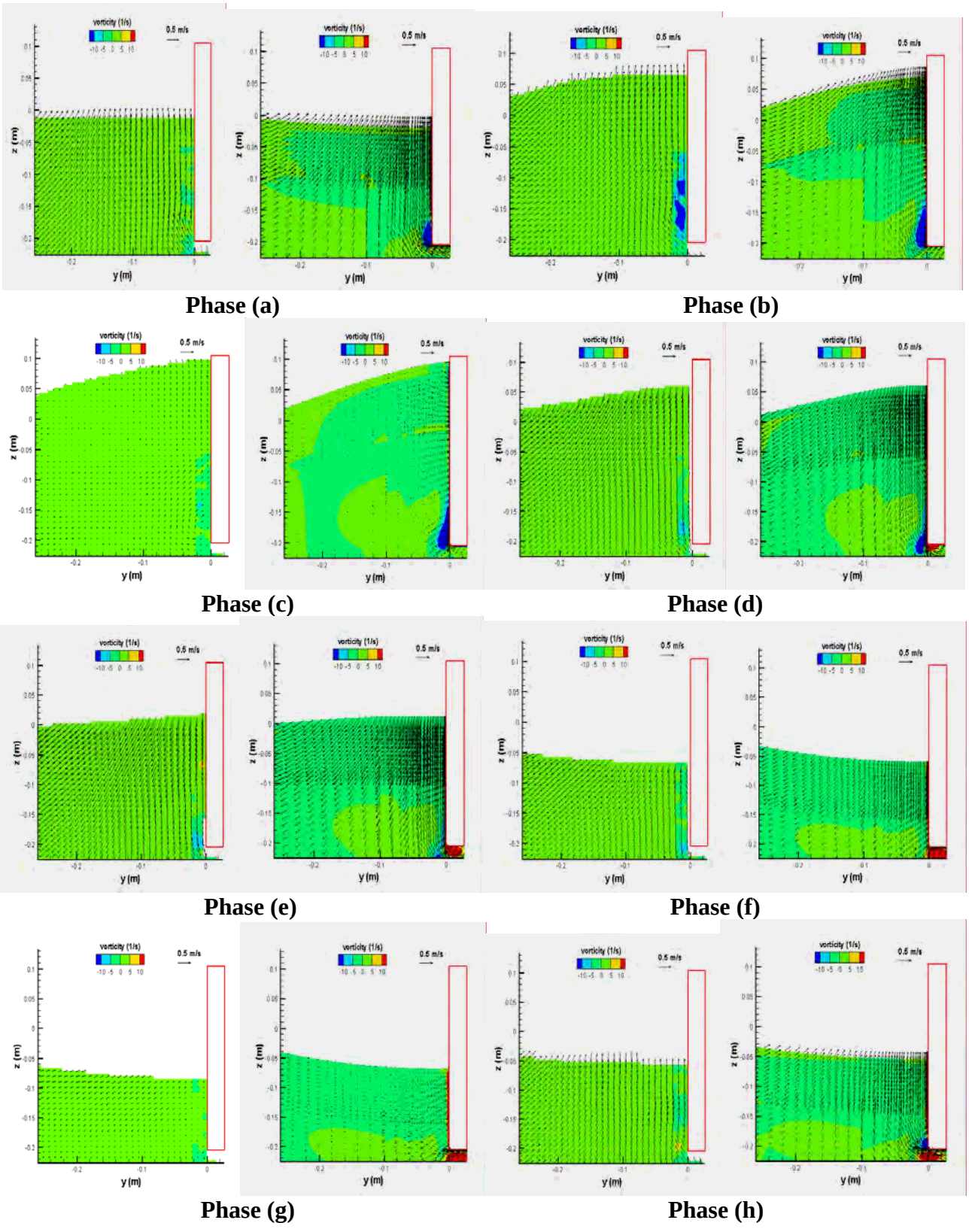

Figure 14: Comparison of measured (left) and calculated (right) vorticity contours and velocity vectors at eight different phases within one wave period; H = 0.175m.

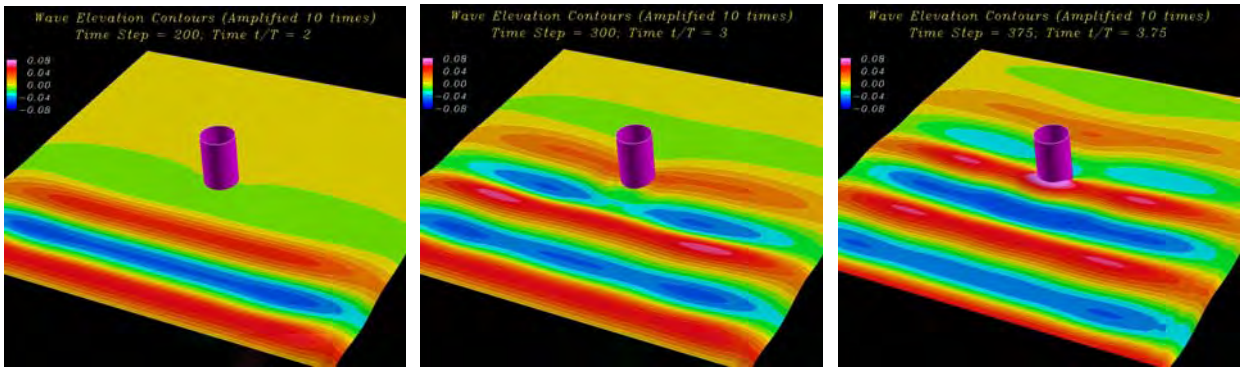

(a) *t/T* = 2.0 **(b) *t/T* = 3.0** **(c) *t/T* = 3.75**

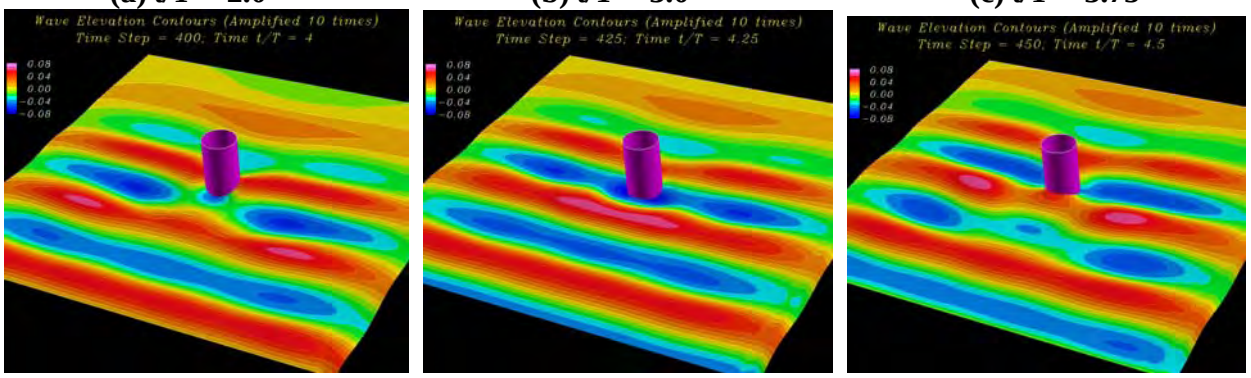

(d) *t/T* = 4.0 **(e) *t/T* = 4.25** **(f) *t/T* = 4.5**

Figure 15: Free surface pressure contours around a single vertical cylinder.

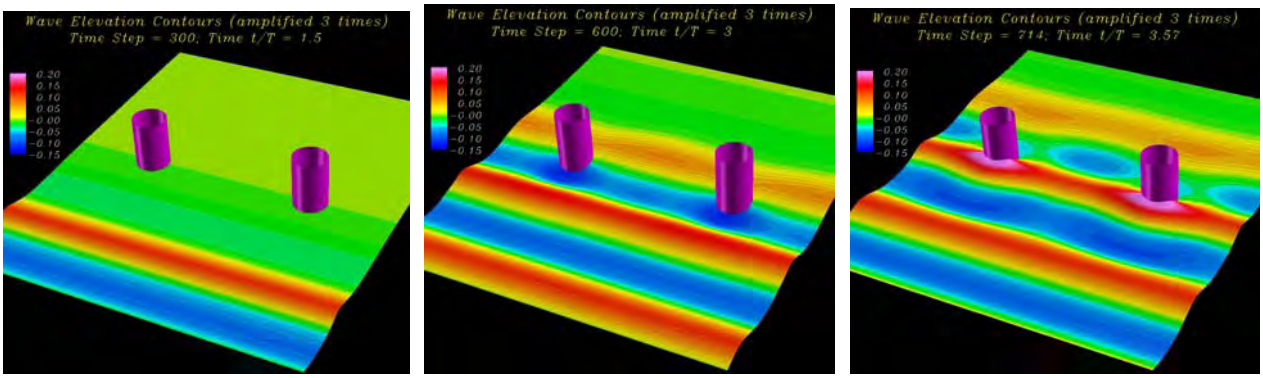

(a) *t/T* = 1.5 **(b) *t/T* = 3.0** **(c) *t/T* = 3.57**

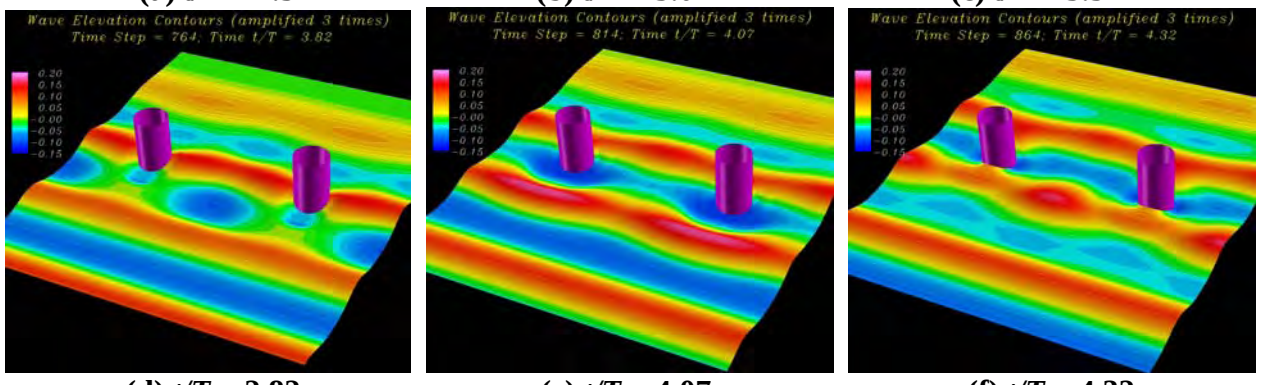

(d) *t/T* = 2.82 **(e) *t/T* = 4.07** **(f) *t/T* = 4.32**

Figure 16: Free surface pressure contours around parallel vertical cylinders.

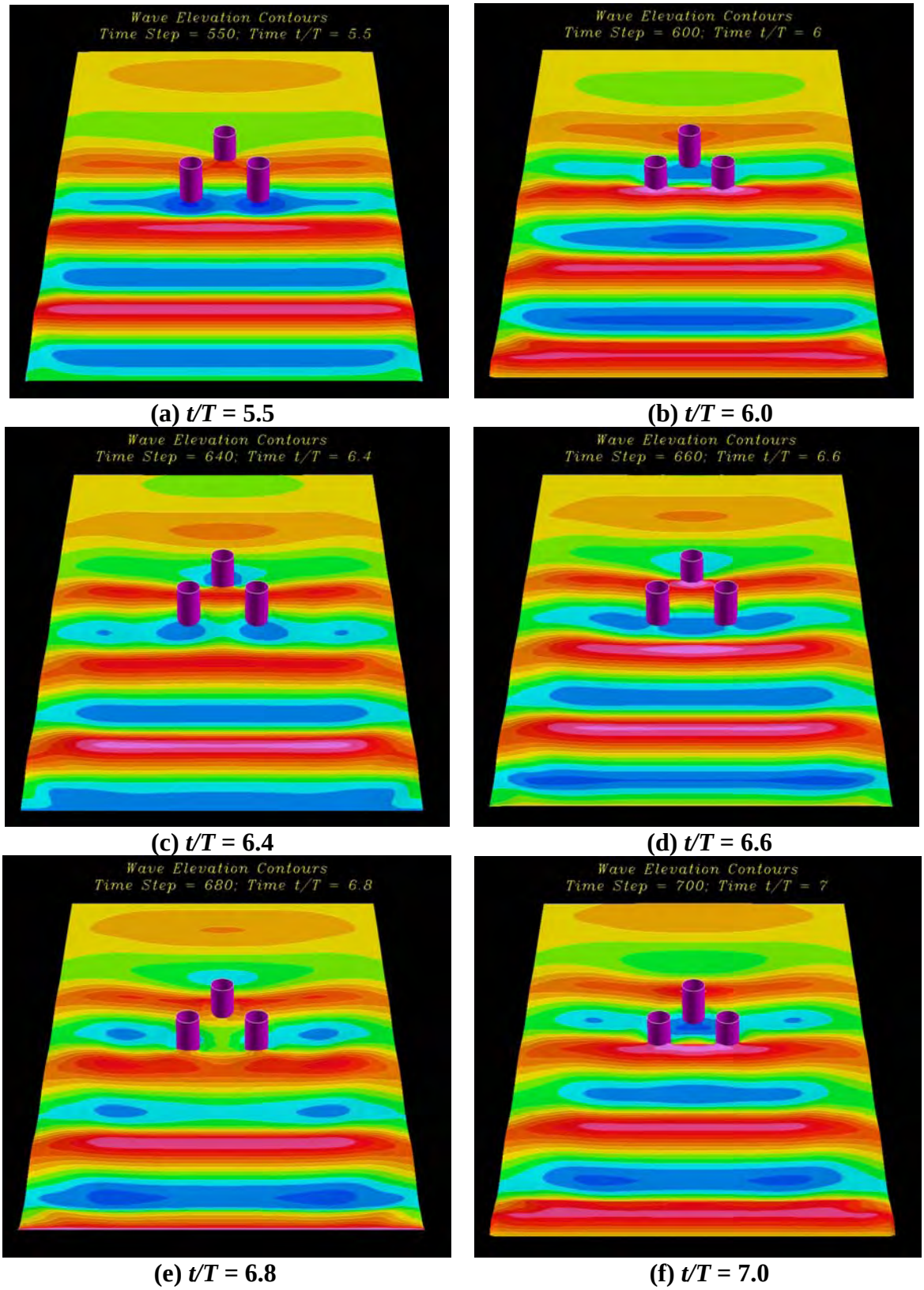

(a) *t/T* = 5.5 **(b) *t/T* = 6.0**

(c) *t/T* = 6.4 **(d) *t/T* = 6.6**

(e) *t/T* = 6.8 **(f) *t/T* = 7.0**

Figure 17: Free surface pressure contours around three cylinders in staggered arrangement.